THE AMERICAN SOCIETY OF MECHANICAL ENGINEERS
Three Park Avenue, New York, N.Y. 10016-5990

99-GT-451

Wake Vorticity Decay and Blade Response in an Axial Compressor with Varying Axial Gap

A.M. Wo
andrew@spring.iam.ntu.edu.tw
Institute of Applied Mechanics
National Taiwan University
Taipei 106, Taiwan
Republic of China

M.H. Chung
Division of Research and Promotion
National Center of High-Performance Computing
Hsinchu, Taiwan
Republic of China

S.J. Chang and **S.F. Lee**
Institute of Applied Mechanics
National Taiwan University
Taipei 106, Taiwan
Republic of China

ABSTRACT

This paper addresses the decay of rotor wake vorticity for a rotor/stator axial compressor, with the axial gap between blade rows being 10, 20 and 30 percent chord, and at both design and high loading levels. Experiments were conducted in a large-scale, low-speed axial compressor. Navier-Stokes calculations were also executed.

Both data and Navier-Stokes results reveal that the decay of rotor wake vorticity increases substantially as the axial gap decreases; the decay for 10 percent gap is about twice that of 30 percent. Increased time-mean blade loading causes the vorticity decay to also increase, with this effect more pronounced for large axial gap than small. At the stator inlet mid-pitch location, the wake maximum vorticity for 10 and 30 percent chord gap cases being nearly the same (differ by 3.8%) at design loading. The corresponding stator unsteady force agrees within 5.2%. Variation of vorticity decay with axial gap is directly linked to the change in potential disturbance by the downstream stator on the rotor wake due to the change in gap spacing. This suggests that the stator potential disturbance causes the upstream rotor wake to decay at an increased rate which, in turns, results in a lowered level of stator response compared to that without this stator/wake interaction effect. Thus, in this context, blade row interaction is considered beneficial.

1.0 INTRODUCTION

Consideration of wakes from turbomachinery blades in the design process cannot be overstated, being self-evident from the extensive research on the subject. There are primarily two tracks in addressing issues related to the blade wake - from the standpoint of machine performance and that of blade

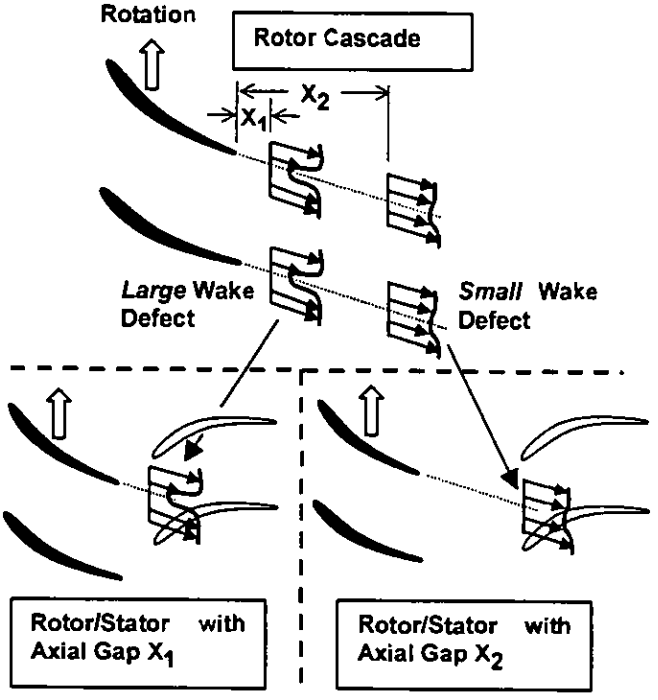

Fig. 1 Misconception of rotor wake decay without consideration of blade row interaction - the downstream stator would ingest approximately the same rotor wake as that from the rotor cascade at the downstream distance the same as the axial gap.

Presented at the International Gas Turbine & Aeroengine Congress & Exhibition
Indianapolis, Indiana — June 7–June 10, 1999

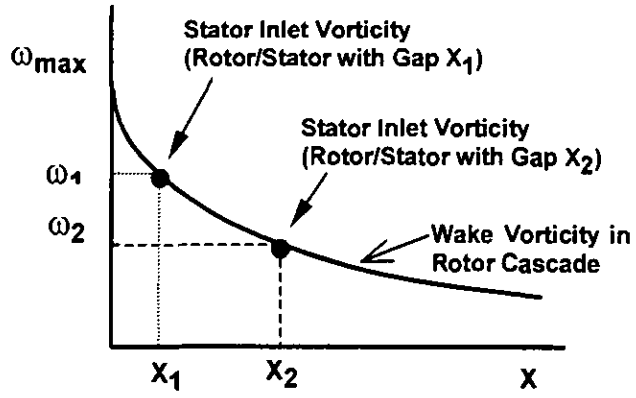

Fig. 2 Wake vorticity decay without consideration of interaction between blade rows, thus the vorticity decay for multi-blade row is approximately the same as that for the cascade configuration.

aeromechanics. The first track mainly focuses on loss of efficiency due to mixing of the wake. Denton (1993) suggested that wake mixing accounts for 20-25% of the total loss in a cascade, and up to 75% of this loss occurred within half of a blade chord downstream of the trailing edge. Since typical axial gap between blade roles is 10-30% of the blade chord, some of this loss can perhaps be recovered. In fact, Smith (1970) first documented a 1% efficiency gain and an increase of 2-7% average stage pressure rise from a three-stage, low-speed compressor rig when the axial gap was decreased from 36.5% chord to 7% chord. Mikolajczak (1977) also found that a decrease in axial gap would increase the efficiency and stage pressure rise. Hetherington and Moritz (1977), however, showed that an *increase* in axial gap would lead to similar results. Smith (1996) recently states that only 25% to 50% of efficiency gain in the 1970 experiment can be attributed to reversible wake attenuation. Thus much work is needed to gain further physical insight. To this end, Valkov (1997) quantified various vortical-disturbance related flow mechanisms that affect the time-averaged compressor performance.

As for aeromechanics concerns, multi-stage turbomachinery blades experience unsteady force either due to self-excited instability or forced response. The first situation arises when a blade extracts energy from the *steady* flow in order to sustain its own unsteady motion. The latter case involves flow disturbances due to the passing of upstream wake, potential effect from upstream and downstream blade rows, and other time varying local flows. Among them, wake is perhaps the most thorny to deal with due to its slow decay rate compared to other mechanisms, and hence has been studied by many researchers. Theoretical work on unsteady disturbances includes Goldstein and Atassi (1976) and Goldstein (1978). Series of experiments (Henderson and Fleeter, 1993a & 1993b; Feiereisen et al., 1993; Weaver and Fleeter, 1994) were conducted by Professor Fleeter and his students on illuminating the physics of vortical and potential disturbances. Gallus et al.

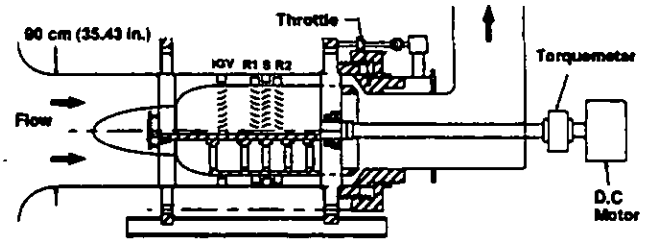

Fig. 3 The experimental compressor rig used in this work.

(1982) also studied potential and wake interactions experimentally. Manwaring and Wisler (1993) provided extensive comparison between the state-of-the-art analysis methods and data on forced response. Chung and Wo (1997) used both Navier-Stokes and panel codes to split the disturbances between blade rows into vortical and potential contributions and Wo et al. (1997) provided details on decomposition of forced response. Hsu and Wo (1998) recently showed that if the blades are clocked properly the potential disturbance from the second rotor row can substantially reduced the upstream stator response caused by wakes from the first rotor blades. This result emphasizes the importance of concrete consideration of blade row interaction.

The motivation of this paper is as follows. Consider the wake downstream of a rotor cascade (top portion of Fig. 1), diffusion and mixing of momentum will cause the wake vorticity to decay. With the addition of a stator row separated by a particular axial gap downstream of the rotor, natural instinct suggests that the stator would ingest vorticity more or less equal to that corresponds to the rotor cascade wake at that axial gap distance downstream (bottom portion of Fig. 1). In other words, the vorticity decay for multi-blade row is approximately the same as that for the cascade configuration. Thus, the larger the axial gap the less the amount of vorticity ingested, as illustrated in Fig. 2. This instinctive thinking, though seems straight-forward, neglected consideration of blade row interaction and, will be shown in this paper, is conceptually incorrect.

2.0 OBJECTIVE

This paper aims to quantify rotor wake vorticity decay for a rotor/stator axial compressor with the axial gap variable between 10% and 30% chord, and to address its effect on the downstream stator unsteady response. Both compressor rig test and Navier-Stokes calculations are undertaken.

3.0 EXPERIMENTAL ASPECTS AND DATA REDUCTION

3.1 Compressor Rig

The experimental compressor is a low-speed, large-scale, one-to-three stage rig, designed after modern compressors (see

	IGV	Rotor (R1 or R2)	Stator
Blade Number	60	58	60
Chord (cm), C	6.00 (2.36in.)	6.00 (2.36in.)	6.00 (2.36in.)
Span (cm), S	8.88 (3.50in.)	8.88 (3.50in.)	8.88 (3.50in.)
Solidity	1.415	1.368	1.415
Tip Clearance (cm)	0.12 (2.0%C)	0.12 (2.0%C)	0.12 (2.0%C)
Aspect Ratio (S/C)	1.48	1.48	1.48
Trailing Edge Radius	1.0 %C	1.0 %C	1.0 %C
Stagger (deg.)	6.58°	-39.50°	20.67°
Camber (deg.)	3.2°	35.0°	48.0°
Inlet Angle, $\beta 1$ (deg.)*	0.0°	56.21°	46.80°
Exit Angle, $\beta 2$ (deg.)*	9.78°	31.03°	4.76°
Diffusion Factor	-	0.407	0.485
Axial Gap (% chord)	175%	variable; see text	
Casing Diameter (cm)		90.0 (35.43 in.)	
Hub/Tip Ratio		0.8	
Mass Flow Coefficient		0.53 to 0.70	
Shaft Speed (RPM)		1050 (max. 1500)	
Reduced Frequency ($\omega C/2C_x$)		7.161	
Mach number (C_x/a)		0.0776	
Reynold's Number at 1050RPM (rotor relative)		1.92×10^5	

* from hot-wire at mid-gap, mid-pitch, for axial gap of 30% chord.

Table 1 General compressor and blade parameters at design condition.

Table 1 and Fig. 3). Flow enters the compressor through a bell-mouth contraction and into the constant blade height annulus. The IGV trailing edge is located 1.75 chord upstream of the rotor leading edge to allow for wake dissipation. The blades were designed using controlled diffusion concept of Hobbs and Weingold (1984). The measured static-to-static pressure rise characteristic (see Hsu and Wo, 1998) is believed to be representative of highly loaded blade of modern design. If not explicitly stated, results reported are taken with the compressor at near-design loading ($\Phi = 0.60$). The blade coordinates and other details of the rig are provided in Hsu and Wo (1998).

3.1 Instrumentation

Unsteady pressure on the stator suction and pressure surfaces were measured using fast-response pressure transducers (Kulite LQ-125), which were embedded within two adjacent blades (10 transducers per surface). The isolated transducer response determines the system response, as calculated from Doebelin (1990). The pressure transducer output was connected to a low-noise amplifier then digitized with a 12-bit analog-to-digital resolution. Transducer signal of 128 data points in a rotor blade-to-blade period was acquired per shaft revolution. The accuracy of the surface pressure measurement is +/- 3% determined from calibration. To provide timing information, a photosensitive diode was used to sense the passing of a metal protrusion rotating with the shaft, with timing accuracy of 0.1% of a blade-to-blade period.

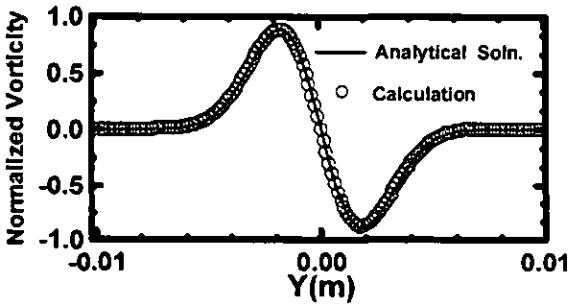

Fig. 4 Comparison of wake vorticity between analytical solution and that discretized using central difference with $\Delta x = \Delta y = 2.9\%$ wake width.

Hsu and Wo (1997) provides details on velocity measurement using the slanted hot-wire technique, with an overall accuracy of +/- 3% in magnitude and +/- 2 degree in flow angles. The hot-wire was located at the stator mid-pitch circumferential direction and was traversed axially, as will be discussed below.

3.3 Vorticity Calculation

Calculation of the vorticity of the rotor wake was based on ensemble-averaged wake data measured in the stationary frame since the vorticity in the relative frame is the same as that in the stationary frame, i.e.,

$$\begin{aligned} \omega_r &= \nabla \times V_r \\ &= \nabla \times (V - V_b) \\ &= \nabla \times V \\ &= \omega \end{aligned}$$

where the subscript r denotes the relative frame, V_b the rotor wheel speed and V the absolute velocity.

Since the ensemble-averaged vorticity is calculated from ensemble-averaged velocity data, thus extreme care is required. First, the ensemble-averaged procedure was scrutinized to determine the suitable number of ensembles so that the ensemble-averaged velocity faithfully represents the velocity field. The number of ensembles tested was 250, 500, 750 and 1,000. The calculated r.m.s. fluctuation, obtained from a time-series data minus its own ensemble-average and take the r.m.s. of the result, is found to depend on the distance of the hot-wire from the rotor trailing edge. Finally 1,000 ensembles was adapted to control the r.m.s. fluctuation within 3% of the mean flow. A total of 197 points hot-wire data were taken within a blade-to-blade period.

Second, the spatial resolution of velocity measurement was determined by the resolution needed to calculate the wake vorticity. An analytical solution of a laminar, far-field wake (White, 1991) originated from an non-lifting airfoil was used to evaluate the spatial resolution, Δx and Δy, needed to compute the vorticity via $\langle \omega \rangle = \partial \langle v \rangle / \partial x - \partial \langle u \rangle / \partial y$ (the symbol $\langle\ \rangle$ denotes an ensemble averaged quantity) with a second-order

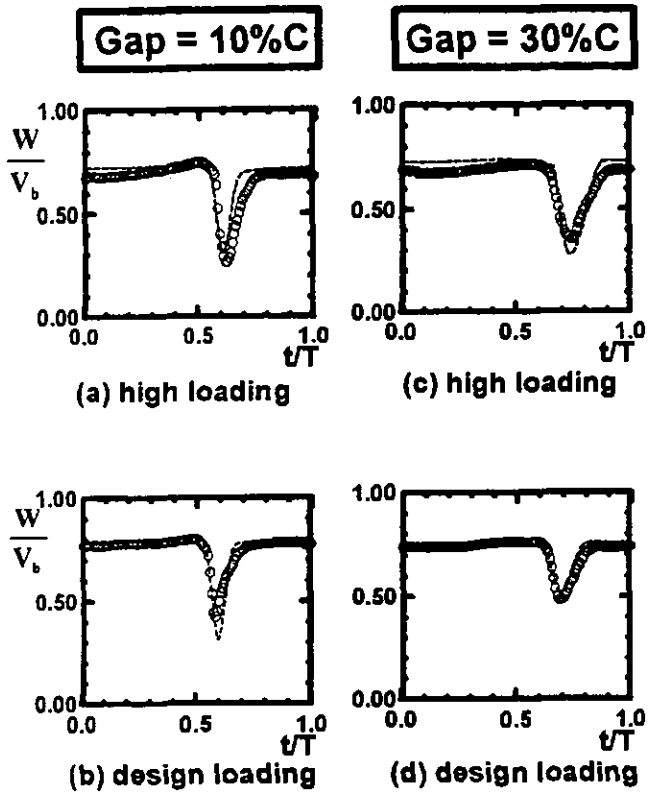

Fig. 5 Comparison of relative velocity (normalized by blade speed) in the rotor wake between Navier-Stokes results (dash lines) and data (symbols) for 10% and 30% chord axial gap cases. Data were taken with hot-wire at *mid-gap* location.

central difference scheme. This vorticity, calculated from velocities at discrete points, was compared with the analytical form of the vorticity distribution. It was found that when Δx = Δy being 2.9% of the wake width the difference in vorticity between the computed and analytical values averaged to be 0.8% of the analytical value, with the range from 0.09% to 2.48%. Figure 4 shows the result of this comparison. Understandably, the largest percentage difference (2.48%) occurs in the outer portion of the wake where the vorticity nearly vanishes. It should be emphasized that the nature of the far-field wake does not affect the evaluation of Δx and Δy since the real importance is the *percentage* of Δx and Δy compared to the wake width. Of course, actual error is higher due to fluctuation in the ensemble-averaged velocity data. In the experiment, Δx = Δy = 2.5% of the wake width was used throughout.

4.0 NAVIER-STOKES CALCULATIONS

To supplement the experimental investigation, a two-dimensional, incompressible, Reynolds-averaged Navier-Stokes code (Chung and Wo, 1997) is used to compute the rotor wake vorticity in the rotor/stator configuration. Governing equations in the blade relative frame are

$$\nabla \cdot \mathbf{u} = 0, \qquad (1)$$

$$\frac{\partial \mathbf{u}}{\partial t} + \nabla \cdot [(\mathbf{u} - \mathbf{u}_b)\mathbf{u}] = -\nabla P + \nabla \cdot [(\mu + \mu_t)\nabla \mathbf{u}], \qquad (2)$$

whre $\mathbf{u}_b$ denotes the rotor speed. The modified Launder-Sharma low-Re version of k-ε two-equation model (Morse, 1991), is used to close the above equations via the eddy viscosity coefficient μ_t. Governing equations used are

$$\frac{\partial k}{\partial t} + \nabla \cdot [(\mathbf{u} - \mathbf{u}_b)k] = \nabla \cdot \left[\left(\mu + \frac{\mu_t}{\sigma_k}\right)\nabla k\right] + G_k - \varepsilon - D \qquad (3)$$

$$\frac{\partial \varepsilon}{\partial t} + \nabla \cdot [(\mathbf{u} - \mathbf{u}_b)\varepsilon] = \nabla \cdot \left[\left(\mu + \frac{\mu_t}{\sigma_\varepsilon}\right)\nabla \varepsilon\right] + C_1 f_{\mu_1} G_k \frac{\varepsilon}{k} - C_2 f_{\mu_2} \frac{\varepsilon^2}{k} + E - F, \qquad (4)$$

where $G_k = \mu_t(\partial u_i/\partial x_k)(\partial u_i/\partial x_k + \partial u_k/\partial x_i)$, $D = 2\mu\left(\partial\sqrt{k}/\partial x_j\right)^2$, $E = 2\mu\mu_t\left(\partial^2 u_i/\partial x_j^2\right)^2$, $F = 2\mu\left(\partial\sqrt{\varepsilon}/\partial x_j\right)^2$, $C_\mu = 0.09$, $C_1 = 1.44$, $C_2 = 1.92$, $\sigma_k = 1.0$, $\sigma_\varepsilon = 1.22$, $f_\mu = \left[1 - \exp\left(-y^+/A^+\right)\right]^2$, $A^+ = 25$, $f_{\mu_1} = 1.0$, $f_{\mu_2} = 1 - 0.21875\exp\left(-R_t^2/36\right)$, with the turbulence Reynolds number $R_t = \rho k^2/(\mu\varepsilon)$, the wall variable $y^+ = \rho y U_\tau/\mu$, and the wall shear velocity $U_\tau = \sqrt{\tau_w/\rho}$.

Equations (1) to (4), in their conservative form as shown, are solved by finite-volume approach using a iterative Semi-Implicit Method for Pressure-Linked Equations (SIMPLE), as developed by Patankar and Spalding (1972). In this work, a non-staggered grid is used with the computation nodes located at the grid cell center. For time discretization, a Crank-Nicolson-like scheme is used to achieve second-order time accuracy. For space discretization, the convection term is approximated by the QUICK scheme (Leonard, 1979) while all other terms use a central difference scheme. The spatial differences are formally second-order accurate.

The computational domain is bounded by various boundaries including inflow/outflow boundaries (located 1.5C upstream of the rotor leading edge and 1.5C downstream of the stator trailing edge, respectively), blade row interface boundaries, periodic boundaries, and rigid blade surfaces. Since there are 58 rotors and 60 stators in the experiment, the calculation is simplified to one rotor and one stator blades with periodic boundaries. Each blade row is discretized using a body-fitted embedded H-type grid. The main reason that the

conventional pinched H-type grid is not used is to avoid an extremely skewed mesh near the blade leading edge. To verify grid independence, two grid sizes were computed - 172x78 cells per row with 108 cells per blade surface and 258x114 cells per row with 160 cells per blade surface. The former grid is found to be satisfactory (Chung, 1995) and is adopted in this work. A slip interface is located at the mid-gap between the two blade rows, which separates two grid systems fixed with respect to each blade. Numerics are passed through the interface as provided in detail in Chung and Wo (1997) and Chung (1995).

Computation is performed using the in-house Cray YMP/EL with four processors. Typical calculation for stator/rotor configuration requires $3x10^{-4}$ CPU second per iteration per cell, with approximately 10 iterations per time step. About 20 to 30 blade-to-blade periods is required from impulsive start to periodic steady state. Thus, the total computational time is about 120 CPU hours.

Figure 5 presents comparison of the wake at the mid-gap location between calculation and data for 10% and 30% axial gap cases and at two blade loading levels. The comparison is fairly good considering that the near-wake flow is still developing. Calculated results for the rotor wake vorticity decay will be presented in Section 5.3.

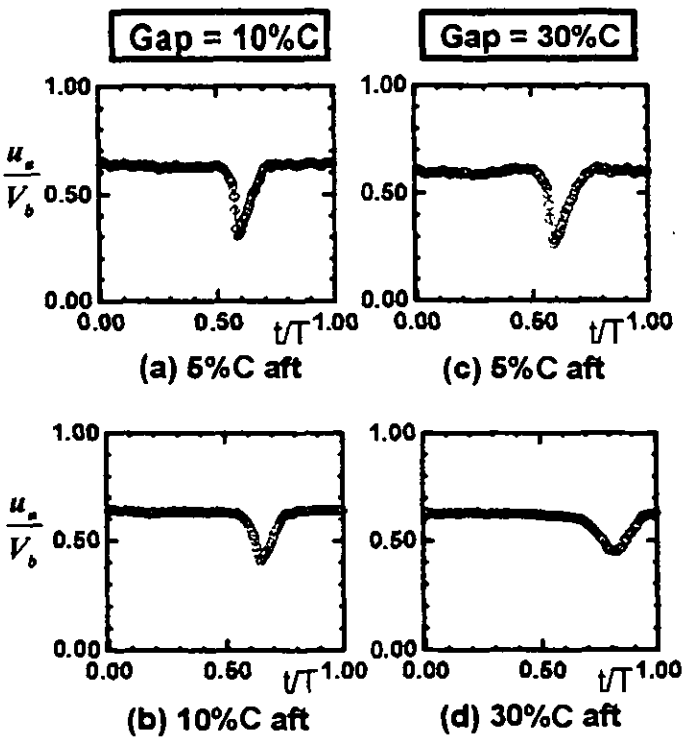

Fig. 6 Rotor wake ensemble-averaged axial velocity data for axial gap of 10% (plot a & b) and 30% chord (plot c & d). (In each sub-figure legend "'X'%C aft" denotes hot-wire located at 'X'% chord aft of the rotor trailing edge in the axial direction along the stator mid-span and mid-pitch line.)

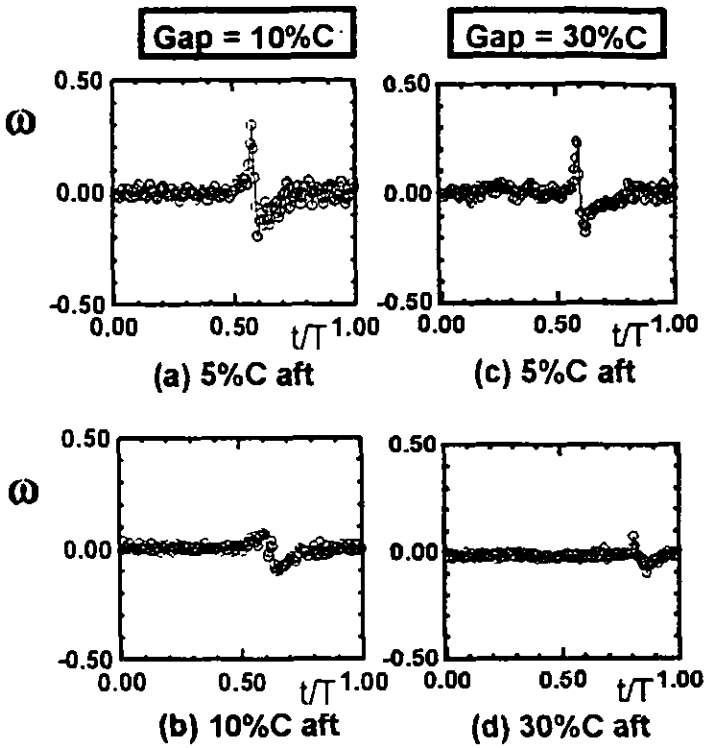

Fig. 7 Ensemble-averaged vorticity which corresponds to ensemble-averaged wake data of Fig. 6.

5.0 RESULTS

5.1 The Unsteady Wake Flow

The ensemble averaged rotor wakes for 10% and 30% chord axial gap cases at near design loading are shown in Fig. 6. For each axial gap, wakes for two axial locations are presented - at 5% chord downstream of rotor trailing edge (hot-wire location closest to the rotor trailing edge) and at the stator leading edge plane. The rotor wake unsteady flow, Fig. 6, reveals a blade wake with the velocity gradient steeper from the pressure surface than that from the suction surface, which is representative of a compressor wake. Diffusion of the wake can be seen by comparing data taken at the two axial locations.

5.2 Vorticity in the Wake

Figure 7 shows the calculated vorticity for the cases of wake data shown in Fig. 6. Within the wake region, vorticity maximum and minimum are due to wake originated from the pressure and suction surfaces, respectively. Note that these peaks are rather well defined. Outside of the wake region vorticity fluctuation about the zero mean is shown, which is much smaller than that within the wake.

Figure 8 presents the maximum vorticity distribution along the axial direction for 10%, 20% and 30% chord axial gap at high loading (Fig. 8a) and near design loading (Fig. 8b).

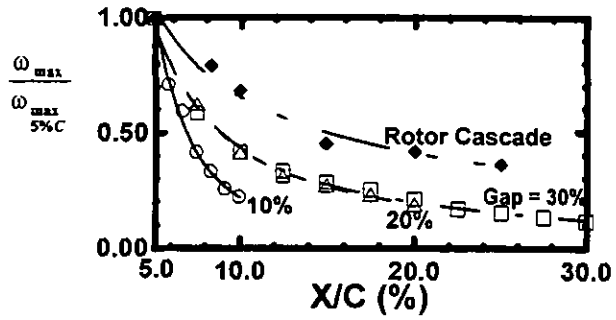

a) High Loading

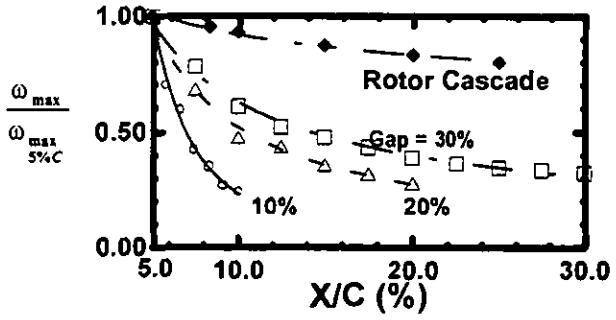

b) Near Design Loading

Fig. 8 Data of axial decay of rotor wake maximum vorticity for axial gap of 10%, 20% and 30% chord cases at high loading (a) and near design (b). (Data normalized by the maximum vorticity at 5% chord aft of the rotor trailing edge - hot-wire location nearest to the rotor.)

There are two reasons to use maximum vorticity (boundary layer from the *pressure* surface) to characterize the wake. First, the spatial variation of minimum vorticity (boundary layer from the *suction* surface) also exhibits similar trend as that for the maximum vorticity - the only difference being vorticity *rise* rather than *decay* - therefore presentation of results on maximum vorticity only is deemed sufficient. Second,

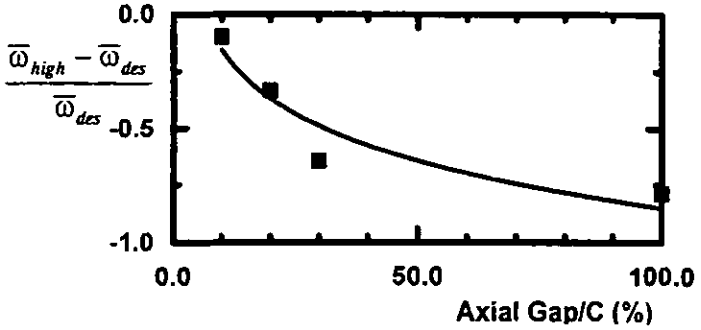

Fig. 9 Difference in the normalized maximum vorticity between high loading and near design with wake at the stator inlet plane. Data (symbols) for 10%, 20%, 30% chord gap and for rotor cascade with wake at one chord aft of rotor trailing edge. Curve fit (solid line) of data is also shown.

calculated value of maximum vorticity is quite well captured, as shown in Fig. 7. The normalization used in Fig. 8 is the maximum vorticity at the hot-wire measurement point closest to the rotor trailing edge, which is 5% chord (3mm) downstream for all axial gap cases. (Numeric values of the maximum vorticity at this 5% chord location for near design loading is 0.301, 0.250 and 0.231 corresponding to 10%, 20% and 30% chord axial gap cases, respectively.)

Unlike that illustrated in Fig. 2 where the wake vorticity follows the same decay for all axial gap cases, Fig. 8 suggests that the general trend of axial decay of vorticity depends strongly on the axial gap - the smaller the axial gap the faster is the spatial decay - *with the decay for 10% gap is at least twice that for 30% gap case.* The vorticity decay is slowest for the isolated rotor configuration, or conceptually the axial gap being infinite as far as blade row interaction is concerned. At the stator inlet, which corresponds to the right-most point for each axial gap case, the normalized vorticity maximum is not much different for all three gap cases. A somewhat perplexing possibility which follows is that a downstream blade row with small axial gap does not necessarily have not to ingest a wake with greater vorticity compared to that with large axial gap. The key issue, therefore, lies in the *spatial rate* of vorticity decay.

At high blade loading, data of Fig. 8a show that vorticity decay for 20% and 30% chord axial gap cases are nearly the same. This can be understood by comparing Fig. 8a with 8b, which suggests that the wake vorticity decay depends on both the axial gap *and* blade loading level. To clarify this point, define the normalized maximum vorticity (ordinate of Fig. 8) at the stator inlet plane as

$$\overline{\omega} \equiv \left.\frac{\omega_{max}}{\omega_{max\ 5\%C}}\right|_{\text{Stator Inlet}}$$

Figure 9 presents the difference in $\overline{\omega}$ between high loading and near design for 10%, 20%, 30% chord gap. For reference purpose, also shown (the right-most point) is the value for rotor cascade wake at one chord aft of the rotor trailing edge as extrapolated from the curve fit of Figs. 8a and 8b. Data show that the difference in $\overline{\omega}$ between high loading and near design increases substantially with axial gap - the difference in vorticity decay between the two loading levels is much smaller for 10% gap than for 30% gap case. Thus the effect of loading on vorticity decay is much more prominent for large gap than for small gap. The overlapping of the vorticity decay for 20% and 30% chord gap (Fig. 8a) essentially is a consequence of this effect.

5.3 Vorticity in the Wake (Navier-Stokes Calculation)

The rotor wake vorticity was also calculated using the Navier-Stokes code as described. The goal of the calculation is to confirm the trend found in Fig. 8b using an entirely

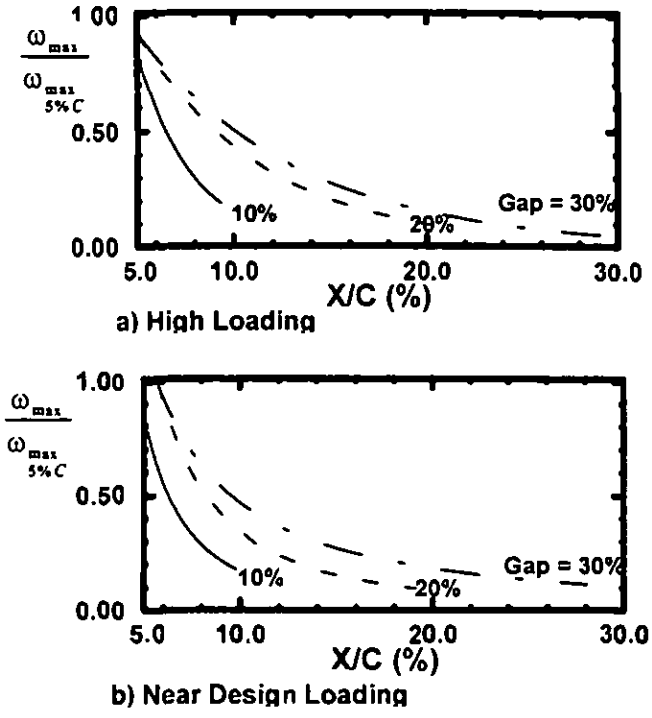

Fig. 10 Navier-Stokes calculated axial decay of rotor wake maximum vorticity for axial gaps of 10%, 20% and 30% chord cases at two loadings. (Numerics normalized by the maximum vorticity at 5% chord aft of the rotor trailing edge.)

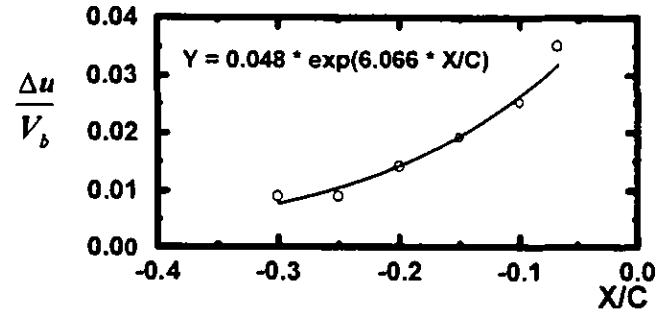

Fig. 11 Difference in axial velocity between the maximum and minimum values as the hot-wire traverses circumferentially upstream of the stator at near design loading. The stator leading edge is located at x= 0. Data (symbols) and curve fit (solid line) are shown.

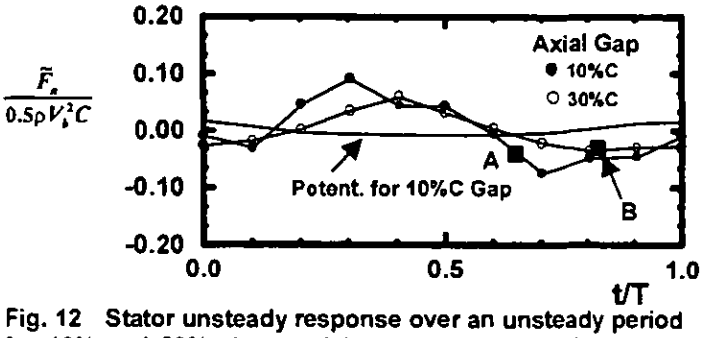

Fig. 12 Stator unsteady response over an unsteady period for 10% and 30% chord axial gap. Also shown (solid line without symbol) is the contribution by the rotor potential disturbance alone on the stator unsteady force for 10% chord gap case.

independent method. Figure 10 presents the results for two loading levels. Although comparison between Fig. 8 (data) and Fig. 10 (calculation) shows that the calculated vorticity is less that of data - the difference primarily due to the difficulty in calculating the vorticity through the rotor/stator interface grid (Chung and Wo, 1997) - the general trend is clearly in accord with each other. That is, Navier-Stokes result further substantiates that the vorticity decay for small gap is faster than that for large gap.

6.0 DISCUSSIONS

6.1 Stator Potential Disturbance on the Rotor Wake

Vorticity decay results of the present work is in agreement with a conclusion from Poensgen and Gallus (1991). They found that the wake of rotating cylindrical rods in an annular cascade decays twice as fast with the downstream stator present than without, thus suggesting that the vorticity decay rate differed for the two configurations studied. However, their aim was not to focus on the effect of variation of the axial gap on vorticity decay thus no such information was provided.

What caused the difference in the vorticity decay for various axial gaps? Physically, the change in the rotor/stator axial gap directly alters the strength of potential disturbance from the downstream stator row on the rotor wake. This potential disturbance has its origin from the surface pressure distribution on the stator blades, which is larger upstream of the stator than downstream since the stator is forward loaded.

To quantify this disturbance, the velocity field of the stator-alone configuration is measured. The rotor/stator axial gap is increased to the hardware limit of *two* chord lengths to allow for the rotor wake to decay, thus essentially achieved the stator cascade configuration. (A hot wire located at the stator inlet plane confirmed that the rotor wake defect is less than 2% of the time-mean flow.) Since a rotating hot-wire is not available to measure the stator upstream potential disturbance as viewed by the rotor wake, a stationary hot-wire is used instead. The disturbance can be obtained by measurement in the stationary frame since the difference in velocity between two points measured by the stationary hot-wire is the same as that by a rotating probe. (That is, V_2-V_1= V_{r2}-V_{r1}, where the subscripts *1* and *2* represent two points in the stationary frame and subscripts *r1* and *r2* denote the same two points as seen in the relative frame.) With the *disturbance* - not the absolute velocity - as our sole interest, this approach allows measurement in the much simpler stationary frame without any compromise in data.

The measurement for the stator potential disturbance is made by incrementally traversing the hot-wire across the entire stator pitch, which is repeated at various axial locations. Figure 11 presents the axial velocity measured upstream of the stator at near design loading. High loading data show almost identical curve as that in Fig. 11, thus the stator potential disturbance on the wake is essentially independent of stator loading. Precisely, the ordinate in the figure represents the difference between the velocity maximum (hot-wire located axially upstream of stator mid-pitch) and minimum (hot-wire located axially upstream of the leading edge) as the stationary hot-wire is incrementally traversed across the stator pitch. The abscissa is simply the distance upstream of the stator, with the stator leading edge located at x= 0. The figure shows that the potential disturbance obeys the well-known exponential decay feature away from the stator, and the disturbance being largest within 30% chord from the leading edge. This level of disturbance is shown to be sufficient to cause the substantial difference in the rotor wake vorticity decay as the axial gap is varied.

6.2 Implication of Rotor Wake Vorticity Decay on Stator Unsteady Loading

How does the rotor wake vorticity decay characteristic of Fig. 8 affects the downstream stator unsteady loading? To answer this question, one needs to first examine the stator unsteady force (obtained by integrating the unsteady pressure data from embedded Kulite gauges in the stator) over one unsteady period for two axial gaps, as presented in Fig. 12 (Hsu and Wo, 1998). Also shown (solid line without symbol) is the stand-alone contribution by the potential disturbance of the rotor towards the total unsteady force on the stator for 10% chord gap, which is decomposed using the procedure described in Wo et al. (1997). (The contribution from 30% chord gap is essentially zero, thus omitted in Fig. 12 for clarity.) The peak-to-peak value of this rotor potential contributed unsteady loading is 15.0% of the *total* unsteady loading for 10% chord axial gap (line with solid symbols). This is relatively small at such close gap spacing since the rotor, like the stator, is also forward-loading thus the potential disturbance by the rotor is much smaller downstream than upstream. In short, the stator unsteady force is dominated by contribution from the rotor wake for all axial gaps studied (also see Hsu and Wo, 1998).

Having established that the stator unsteady loading signature is mainly due to the rotor wake alone, the rotor wake vorticity decay characteristic (Fig. 8) can now be linked to the stator unsteady force (Fig. 12). Data of Fig. 8 was taken with the hot-wire located at the stator mid-pitch position (mid-way between two adjacent stators) traversing axially. When the hot-wire is at the stator leading edge plane, Figs. 6b and 6d show the maximum wake defect occurs at non-dimensional time t/T = 0.64 for 10% chord axial gap and t/T = 0.81 for 30% chord axial gap, respectively. This time delay is due to the combined effect of the rotor stagger angle and the difference in axial gap. (Note that t/T = 0.5 corresponds to the rotor trailing edge being axially upstream of the stator mid-pitch position.) At the stator leading edge plane, Fig. 8b suggests that dimensional value of maximum vorticity ω_{max} is 0.0726 (= 0.241* 0.301, with 0.301 being the value used for normalization) for 10% chord axial gap and 0.0754 (= 0.326* 0.231, with 0.231 being the value used for normalization) for 30% chord axial gap case, which differs by only 3.8%. In other words, for the two axial gap cases, the rotor wake maximum vorticity is essentially the same at the stator leading edge plane at the instant when the wake arrives at the hot-wire.

To link the same rotor wake vorticity at the stator inlet plane to the stator unsteady force for the 10% and 30% chord gap cases, Fig. 12 shows that at t/T= 0.64 for 10% chord gap the normalized unsteady force is -0.0423 (Point A solid square in Fig. 12) and at t/T= 0.81 for 30% chord gap the normalized unsteady force is -0.0354 (Point B solid square in Fig. 12). Thus, the two values differs by 0.0069. With the average of the peak-to-peak force amplitude for the two gaps being 0.133, a difference of 0.0069 implies a mere 5.2% of the average peak-to-peak amplitude, which is comparable to the percentage difference in the vorticity maximum of 3.8% at the stator inlet. Hence, the stator unsteady response can be directly related to the rotor wake vorticity decay, since the rotor potential contribution is negligible.

One might be curious of the fundamental reason why the vorticity maximum can be related to the unsteady stator force as described. After all, the unsteady blade force is an integrated quantity with contributions from unsteady pressure on the *entire* blade. The answer lies in that the dominant contribution to the unsteady pressure (a pressure spike) occurs *locally* near the leading edge region when the upstream wake hits the stator. This fact has been concretely demonstrated by Hsu and Wo (1988) with its usage in reducing the stator unsteady force via rotor clocking.

6.3 Isolated Blade Row Analysis

Present results suggest that isolated blade row analysis, i.e. *wake/blade* calculation with the rotating wake as the inlet boundary condition to a stationary blade row, must use the wake from *blade/blade* configuration at the computational inlet (with the downstream blade equivalent to that in the isolated blade row study and at the same loading level). This is because the use of a wake with arbitrary defect and wake width at the inlet boundary, or even the wake from upstream blade row cascade, does not necessarily correspond to any particular blade/blade configuration, since the evolution of the wake depends strongly on the axial gap between blade rows, and blade loading, as discussed. Once a wake profile is prescribed at the inlet plane, the potential field of the downstream blade row dominates its vorticity decay characteristic. However, the need of a blade/blade calculation to obtain the inlet wake for an isolated blade row analysis seems to violate basic motivation

for such analysis, namely to save computational cost.

6.4 Rotor/Stator Count

If the rotor/stator blade count were significantly different than that in this work (58/60), major results found would still hold, namely vorticity decay depends strongly on the axial gap and blade loading. The key issue is the distance between a particular upstream wake to the nearby stators, since it is the stator potential disturbance which causes the vorticity decay characteristic as discussed. And this distance depends on the rotor/stator blade count.

7.0 CONCLUSIONS

Experimental and numerical studies are conducted on the rotor/stator axial compressor with the goal of quantifying the rotor wake vorticity decay and its consequence on the stator response. Major results include

- Both rig test and Navier-Stokes calculation confirm that the decay of maximum vorticity increases substantially as the axial gap decreases.
- The decay for 10 percent chord gap is at least twice that for 30 percent gap.
- As time-mean blade loading increase, wake vorticity decay also increase. This increase is greater for large gap than for small gap.
- For 10 and 30 percent gap cases at near design loading, the rotor wake vorticity maximum at the stator inlet mid-pitch location differs by only 3.8%.
- At this time instant, the stator unsteady force differs by a comparable magnitude of 5.2% for the two gaps. Thus the vorticity decay can be related to the blade response.
- As the axial gap varies, the difference in the rotor vorticity decay is fundamentally a result of the difference in the potential disturbance by the downstream stator row on the rotor wake.
- Since the rotor wake vorticity decay increases as axial gap decreases, the stator potential disturbance causes the upstream wake to decay at an increased rate which, in turn, results in a lowered level of its own blade response compared to that without this stator/wake interaction effect.
- Thus, this form of blade row interaction is beneficial from the point of view of stator unsteady response.

ACKNOWLEDGEMENTS

The authors are grateful to the reviewers for their thoughtful comments. Financial support from the National Science Council, Republic of China (Grant No. NSC 86-2612-E-002-009) is appreciated. The first author also acknowledges the help of Christ in this work.

REFERENCES

Chung, M.H., 1995, "Numerical Study of Vortical and Potential Disturbances and Gust Response in an Axial Compressor," Doctoral thesis, Institute of Applied Mechanics, National Taiwan University, Taipei, Taiwan, Republic of China.

Chung, M.H. and Wo, A.M., 1997, "Navier-Stokes and Potential Calculations of Axial Spacing Effect on Vortical and Potential Disturbances and Gust Response in an Axial Compressor," *ASME J. of Turbomachinery*, Vol. 119, pp. 420-428.

Denton, J.D., 1993, "Loss Mechanisms in Turbomachines," *ASME J. Turbomachinery*, Vol. 115, No. 4.

Doebelin, E.O., 1990, Measurement Systems: Application and Design, 4th ed., McGraw-Hill, p. 482.

Feiereisen, J.M., Montgomery, M.D. and Fleeter, S., 1993. "Unsteady aerodynamic forcing functions: a comparison between linear theory and experiment," *ASME paper 93-GT-141*.

Gallus, H.E., Groillus, H., and Lambertz, J., 1982, "The Influence of Blade Number Ratio and Blade Row Spacing on Axial-Flow Compressor Stator Blade Dynamic Load and Stage Sound Pressure Level," *J. Eng. for Power*, Vol. 104, pp. 633-644.

Giles, M.B., 1988, "Calculation of unsteady wake/rotor interaction," *J. of Propulsion and Power*, Vol. 4. pp. 356 - 362.

Goldstein, M.E. and Atassi, H., 1976, "A complete second-order theory for the unsteady flow about an airfoil due to periodic gust," *Journal of Fluid Mechanics*, Vol. 74, part 4: pp. 741-765.

Goldstein, M.E., 1978, "Unsteady vortical and entropic distortions of potential flows round arbitrary obstacles," *Jaurnal of Fluid Mechanics*, Vol. 89, part 3, pp. 433-468.

Hall, K. and Crawley, E., 1989, "Calculation of unsteady flows in turbomachinery using the linearized Euler equations," *AIAA J.*, Vol. 27, No. 6, pp. 777 - 787.

Henderson, G. and Fleeter, S., 1993, "Forcing function effects on unsteady aerodynamic gust response: part 1- forcing functions," *J. of Turbomachinery*, Vol. 115, pp. 741-750.

Henderson, G. and Fleeter, S., 1993, "Forcing function effects on unsteady aerodynamic gust response: part 2 - low solidity airfoil row response," *J. of Turbomachinery*, Vol. 115, pp. 751-761.

Hobbs, D.E. and Weingold, H.D., 1984, "Development of controlled diffusion aerofoils for multistage compressor applications." *J. Eng. for Gas Turbine & Power*, Vol. 106, pp. 271-278.

Hetherington, R. and Moritz, R.R., 1977, "The Influence of Unsteady Flow Phenomena on the Design and Operation of Aero Engines," in "Unsteady Phenomena in Turbomachinery," AGARD CP-144.

Hsu, S.T., Wo, A.M. and Wu, C.K., 1996, "Experimental and Numerical Study of Gust and Gust Response in a Rotor/Stator Axial Compressor," presented in the ASME Turbo Asia '96, Jakarta, Indonesian, *ASME Paper 96-TA-043*.

Hsu, S.T. and Wo, A.M., 1997, "Near-Wake Measurement in a Rotor/Stator Axial Compressor using Slanted Hot-wire Technique," *Experiments in Fluids*, Vol. 23, pp. 441-444.

Hsu, S.T. and Wo, A.M., 1998, "Reduction of Unsteady Blade Loading by Beneficial Use of Vortical and Potential Disturbances in an Axial Compressor with Rotor Clocking," ASME *J. of Turbomachinery*, Vol. 120, No. 4, pp. 705-713.

Kerrebrock, J.L., 1992, Aircraft Engines and Gas Turbines, 2nd Ed., M.I.T. Press, p. 371.

Leonard, B.P., 1979, "A stable and accurate convective modeling procedure based on quadratic upstream interpolation," *Computer Methods in Applied Mechanics and Engineering*, Vol. 12, pp. 59-98.

Manwaring, S.R. and Wisler, D.C., 1993, "Unsteady aerodynamics and gust response in compressors and turbines," *J. of Turbomachinery*, Vol. 115, pp. 724 - 740.

Mikolajczak, A.A., 1977, "The Practical Importance of Unsteady Flow," in "Unsteady Phenomena in Turbomachinery," in AGARD CP-144.

Morse, A.P., 1991, "Application of a low Reynolds number turbulence model to high-speed rotating cavity flows," *J. of Turbomachinery*, Vol. 113, pp. 98-105.

Patankar, S.V. and Spalding, D.B., 1972, "A calculation procedure for heat, mass and momentum transfer in three-dimensional parabolic flows," *International J. of Heat and Mass Transfer*, Vol. 15, pp. 1787-1797.

Poensgen, C. and Gallus, H.E., 1991, "Three-Dimensional Wake Decay Inside of a Compressor Cascade and Its Influence on the Downstream Unsteady Flow Field. Part I - Wake Decay Charactheristics in the Flow Passage," ASME *J. of Turbamachinery*, Vol. 113.

Smith, L.H., 1996, Discussion of *ASME Paper 96-GT-029.*

Smith, L.H., 1970, "Casing Boundary Layers in Multistage Axial Flow Compressors," Flow Research on Blading, L.S. Dzung (ed.), Elsevier Publishing Company.

Valkov, T., 1997, "The Effect of Upstream Rotor Vortical Disturbances on the Time-Average Performance of Axial Compressors Stators," M.I.T. Gas Turbine Lab Report No. 227.

Valkov, T. and Tan, C.S., 1995, "Control of the Unsteady Flow in a Stator Blade Row Interacting with Upstream Moving Wakes," *J. of Turbomachinery*, Vol. 117, pp. 97 - 105.

Weaver, M.M. and Fleeter, S., 1994, "Turbine Rotor Generated Forcing Functions for Flow Induced Vibrations," *ASME paper 94-GT-328.*

Wo, A.M., Chung, M.H. and Hsu, S.T., 1997, "Gust Response Decomposition in a Stator/Rotor Axial Compressor with Varying Axial Gap," *J. of Prop. and Power*, Vol. 13, No. 2, pp. 178-185.

White, F.M., 1991, Viscous Fluid Flow, second edition, McGraw Hill.